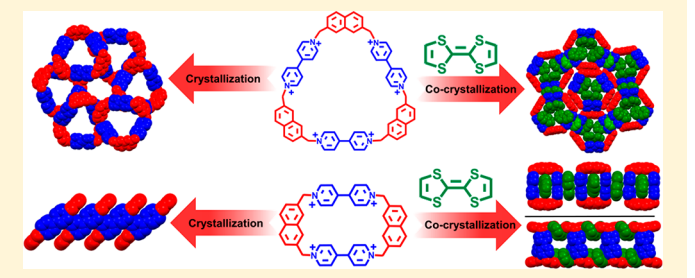


# Combining Intra- and Intermolecular Charge Transfer with Polycationic Cyclophanes To Design 2D Tessellations

Supporting Information

ABSTRACT: A series of donor-acceptor (D-A) naphthalene-viologen-based cyclophanes of different shapes, sizes, and symmetries have been synthesized and characterized. Solution optical studies on these cyclophanes reveal the existence of photoinduced intramolecular charge transfer (CT) at 465 nm from naphthalene (D) to viologen (A) units, resulting in a conformational change in the viologen units and the emergence of an emission at 540 nm. The D-A cyclophanes with box-like and hexagon-like shapes offer an opportunity to control the arrangement within 2D layers



where D-A interactions direct the superstructures. While a box-like 2,6-disubstituted naphthalene-based tetracationic cyclophane does not form square tiling patterns, a truncated hexagon-like congener self-assembles to form a hexagonal superstructure which, in turn, adopts a hexagonal tiling pattern. Tessellation of the more rigid and highly symmetrical 2,7disubstituted naphthalene-based cyclophanes leads to the formation of 2D square and honeycomb tiling patterns with the boxlike and hexagon-like cyclophanes, respectively. Co-crystallization of the box-like cyclophanes with tetrathiafulvalene (TTF) results in the formation of D-A CT interactions between TTF and viologen units, leading to tubular superstructures. Cocrystallization of the hexagon-like cyclophane with TTF generates well-ordered and uniform tubular superstructures in which the TTF-viologen CT interactions and naphthalene-naphthalene  $[\pi \cdots \pi]$  interactions propagate with 2D topology. In the solid state, the TTF-cyclophane co-crystals are paramagnetic and display dual intra- and intermolecular CT behavior at ~470 and ~1000 nm, respectively, offering multi-responsive materials with potential pathways for electron transport.

## INTRODUCTION

Over the past three decades, two-dimensional (2D) networks of polygons with uniform or heterogeneous morphologies have attracted considerable attention owing to the physical properties generated by their morphologies, as well as their porous architectures.<sup>2</sup> The regular arrangement of matching shapes to cover completely a plane, without overlaps or gaps, is known as tessellation. This process has been used to tile regular polygons for decoration and art since antiquity. The mathematical treatment, however, of tiling regular polygons of triangular, square, and hexagonal shapes was first reported<sup>4</sup> in 1619 by Kepler, who identified only 11 types of Archimedean tilings (ATs), including three regular and eight semi-regular tiling modes. Manifestations of Archimedean tiling have been observed in the bulk structure of metallic alloys and supramolecular interfacial tessellations, liquid crystals, polymer systems,<sup>8</sup> and systems of patchy nanocrystals.<sup>9</sup> Recent

studies by Glotzer et al.10 have revealed the influence of entropic and enthalpic factors on the self-assembly of Archimedean tilings. Several materials forming Archimedean tiles exhibit striking photonic, 11 electronic, 12 and diffusive properties. 13

Tessellations have also been used to build beautifully designed crystalline porous 2D frameworks through the judicious connection of building blocks as vertices and edges into an extended plane.2 Tessellation of a certain type of monomeric vertices results in regular polygons in covalent organic frameworks (COFs). The stacking of these planar superstructures leads to the formation of molecular channels in one dimension. The first COF structure was reported by Yaghi<sup>14</sup> in 2005; since then, organic materials with uniform

Received: July 23, 2019 Published: October 3, 2019



<sup>&</sup>lt;sup>†</sup>Department of Chemistry and <sup>||</sup>Institute for Sustainability and Energy at Northwestern (ISEN), Northwestern University, 2145 Sheridan Road, Evanston, Illinois 60208-3113, United States

<sup>&</sup>lt;sup>¥</sup>Joint Center of Excellence in Integrated Nanosystems, King Abdulaziz City for Science and Technology, Riyadh 11442, Kingdom of Saudi Arabia

<sup>&</sup>lt;sup>§</sup>Institute of Molecular Design and Synthesis, Tianjin University, 92 Weijin Road, Nankai District, Tianjin 300072, P. R. China  $^{\perp}$ School of Chemistry, University of New South Wales, Sydney, NSW 2052, Australia

pore structures have been studied extensively. These 2D polymers have shown several applications, such as gas storage and separation, <sup>15</sup> heterogeneous catalysis, <sup>16</sup> optoelectronic materials, <sup>17</sup> and ion conduction. <sup>18</sup> In contrast to COFs with regular tessellation arrangements affording a single pore type, the use of different building blocks results in unsymmetrical edges, which generate irregular polygons. Tessellation of these irregular polygons creates COFs with several different pore types. Zhang et al. 19 reported two porous 2D COFs with periodically heterogeneous pore structures synthesized through a desymmetrized vertex design strategy. The development of multi-porous COFs, however, remains challenging owing to the strong tendency toward polymorphism.<sup>12</sup> Multi-porous COFs have the potential for an extraordinary range of applications, such as control of semiconducting electrontransport properties by judicious electron-hole doping, or simultaneous uptake and transportation of different guests.<sup>20</sup>

Other approaches that have been adopted in the design of 2D porous materials include supramolecular tiling of diagonal, trigonal, or tetragonal building blocks carrying different functional groups designed to form noncovalent intermolecular linkages by hydrogen bonding, van der Waals interactions, or coordination to metal centers.  $^{21}$  For instance, Miyata et al.  $^{22}$ reported that a  $C_3$ -symmetric and  $\pi$ -conjugated macrocycle combined with an appropriate hydrogen-bonding module allows the construction of crystalline supramolecular frameworks with a cavity volume of up to 58%. The frameworks were obtained through non-interpenetrated stacking of a hexagonal sheet possessing three types of pores with different sizes and shapes. The void space is rather fragile, however, and can be affected by several factors, such as solute concentration, temperature, solvent polarity, and the presence of guest molecules.<sup>23</sup> Other approaches, <sup>24–26</sup> which consist of tiling shape-persistent polygonal macrocycles leading to the construction of 2D porous materials, have attracted considerable attention. Several triangular systems decorated with long alkyl chains have been employed<sup>24</sup> in the construction of 2D glassystate networks. While other studies<sup>25</sup> have demonstrated the emergence of chiral multi-component supramolecular networks formed by achiral molecules at the interface of a chiral solvent and an achiral substrate, a more recent investigation describes<sup>26</sup> the hexagonal tiling of hexagonal macrocycles of different sizes through a combination of hydrogen-bonding and van der Waals interactions to form a periodically ordered 2D network at the liquid-solid interface.

Polycationic cyclophanes constitute another family of macrocycles that have attracted significant attention in the past three decades. The synthetic availability and desirable electronic properties of 1,1'-disubstituted-4,4'-bipyridinium and its derivatives have, to a large extent, driven research in this area and generated numerous cyclophanes in this family. Several rigid polycationic box-like cyclophanes with different shapes, sizes, and electronic properties have been synthesized with a number of desirable properties, including (i) host—guest recognition and complexation, (ii) catalysis, (iii) artificial photosystems, (iv) molecular electronics, (iv) live-cell imaging and therapy, (iv) molecular machines.

Our design approach (Figure 1a) for the tessellation of polycationic cyclophanes consists of the combination of donor (D) and acceptor (A) electroactive building blocks in a single macrocycle. Beyond the enhancement of the intramolecular charge transfer compared to phenylene-based viologen cyclophanes, <sup>28</sup> the intermolecular D-A interactions between macro-

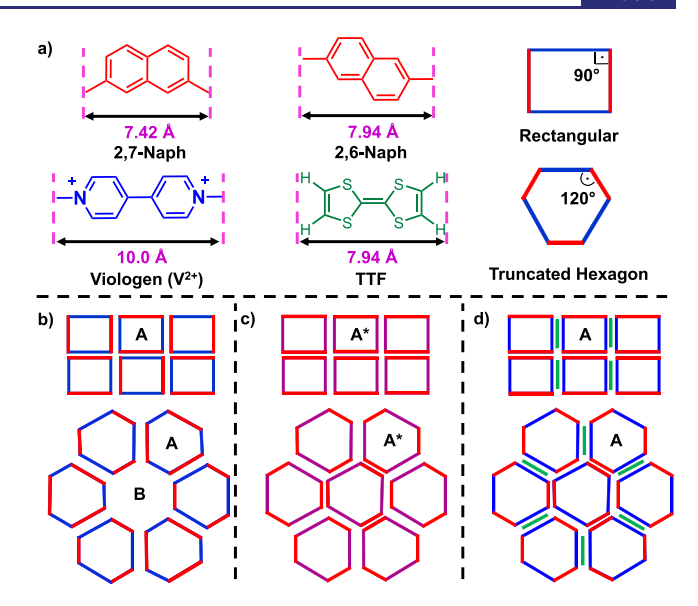


**Figure 1.** (a) D-A building blocks for the design of truncated polygons using 2,7-naphthalene, 2,6-naphthalene, and viologen, with tetrathiafulvalene (TTF) between polygons. Expected tiling of polygons via (b) D-A interactions (represented by A), (c) radicalradical pairing interactions (A\*), and (d) CT interactions in TTF-cyclophane co-crystals. Color-coded representations: red for either a 2,6- or 2,7-naphthalene unit, blue for dicationic viologen units, purple for viologen radical units, and green for TTF units. The symbol B represents a secondary space formed by D-A interactions.

cycles are expected to be the structure-directing interactions governing the creation of 2D networks. Recently we reported the tessellation of electron-active naphthalene diimide cyclophanes of triangular shape (NDI- $\Delta$ ) through  $[\pi\cdots\pi]$  and D-A CT interactions that offer different triangular and hexagonal tiling patterns, depending on the crystal growth conditions. While in our last investigations we exploited the electron-sharing character within NDI- $\Delta$  to offer additional degrees of freedom for electron transport in 2D tessellated CT networks, in the current work, we are exploiting combinations of the intra- and intermolecular CT in cyclophanes in order to construct CT materials with 2D topologies. Furthermore, tessellation of irregular shape-persistent polygons to create 2D networks by using weak interactions remains underexplored.

Here, we report the use of rigid D-A cyclophanes with different sizes, shapes, and symmetries to construct a range of 2D D-A networks, as shown in Figure 1a. The differences in the lengths of 2,7- and 2,6-disubstituted naphthalene units and viologen, when combined, allow the creation of truncated polygons. The local  $C_{2\nu}$  and  $D_{2h}$  symmetries of 2,7- and 2,6disubstituted naphthalene units, respectively, affect the rigidity, shapes, and symmetries of these cyclophanes. While the local  $D_{2h}$  symmetry of the 2,6-disubstituted naphthalene unit is expected to generate a macrocycle with  $D_{3h}$  symmetry, the local  $C_{2\nu}$  point group symmetry of the 2,7-disubstituted naphthalene unit can result in truncated hexagon-like macrocycles resulting from the different conformations adopted by the naphthalene units. The interactions between the relatively electron-rich naphthalene units (D) and electron-poor viologen units (A) are expected (Figure 1b) to be the structure-directing interactions.

The molecular arrangements can be tailored by changing the redox state of the viologen units. Indeed, upon reduction (Figure 1c) of the viologen units to viologen radicals, the

packing in the solid state will be rather dictated by the radicalradical pairing of the viologen radical units. Moreover, cocrystallization of cyclophanes with a stronger electron-donor guest molecule, such as TTF (Figure 1d), is expected to generate TTF-viologen CT interactions, which will propagate in 1D and 2D in the case of box-like and hexagon-like structures, respectively. In addition, the confinement of TTF in porous materials has been proven to enhance the CT behavior.<sup>35</sup> All these design rules can facilitate the creation of programmable building blocks with well-defined crystal habits. Absorption and emission studies have been undertaken to unravel the optical properties of all the cyclophanes in solution, along with <sup>1</sup>H nuclear magnetic resonance (NMR) titrations to calculate the affinities of the different cyclophanes to TTF as the guest molecule. Single-crystal X-ray studies of all cyclophanes provided detailed information about the molecular structures and packings in the solid state.

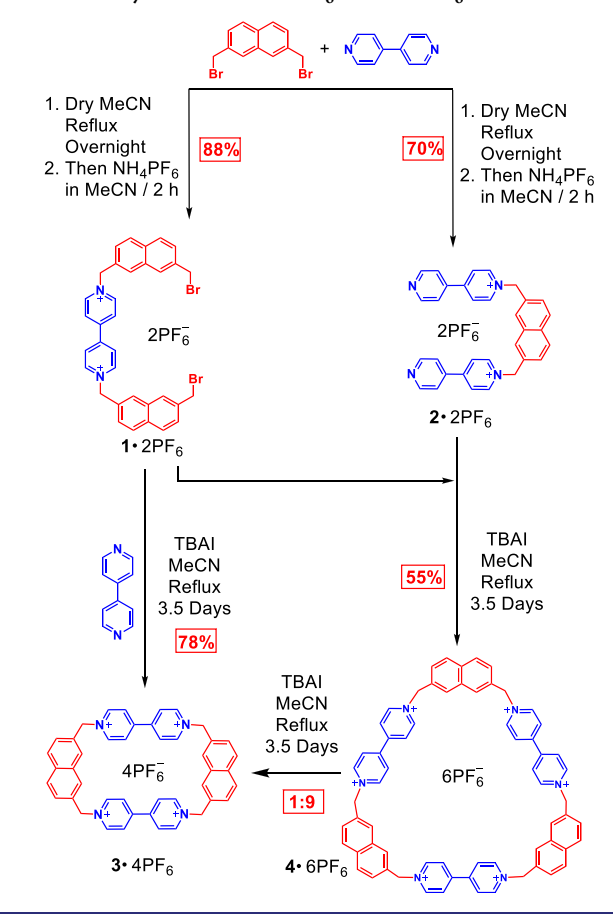
## ■ RESULTS AND DISCUSSION

**Synthesis.** The syntheses of the cyclophanes 3.4PF<sub>6</sub>, 4. 6PF<sub>6</sub>, 7·4PF<sub>6</sub>, and 8·6PF<sub>6</sub> are described in Scheme 1 and Scheme 2. All the cyclophanes were synthesized without the use of templates. The reactions of 1·2PF<sub>6</sub> with 2·2PF<sub>6</sub> and of 5· 2PF<sub>6</sub> with 6·2PF<sub>6</sub> in a 1:1 ratio in dry MeCN and in the presence of ~5 mol% 'Bu<sub>4</sub>NI under refluxing conditions were followed by the addition of excess of NH<sub>4</sub>PF<sub>6</sub> in order to effect complete counterion exchange. After being washed with deionized H2O and CH2Cl2, the filtered crude solid was subjected to reverse-phase column chromatography, affording 4.6PF<sub>6</sub> (55%) and 8.6PF<sub>6</sub> (60%), respectively. A combination of <sup>1</sup>H and <sup>13</sup>C (NMR) spectroscopy and high-resolution mass spectrometry (HRMS) confirmed (Figures S1-S20) the formation of both 4.6PF<sub>6</sub> and 8.6PF<sub>6</sub>. Similarly, the reactions of 1.2PF<sub>6</sub> or 5.2PF<sub>6</sub> and 4,4'-bipyridine in a 1:8 ratio in dry MeCN and in the presence of ~5 mol% <sup>t</sup>Bu<sub>4</sub>NI under refluxing conditions were followed by the addition of excess NH<sub>4</sub>PF<sub>6</sub> in order to effect complete counterion exchange. After being washed with H2O and CH2Cl2, the filtered crude solid was subjected to reverse-phase column chromatography, affording 3.4PF<sub>6</sub> (78%) or 7.4PF<sub>6</sub> (72%). (see Supporting Information for more details).

The synthesis of  $4.6PF_6$  also afforded  $3.4PF_6$  as a byproduct with a yield of 14%. This result suggested a possible conversion of  $4.6PF_6$  to  $3.4PF_6$ . Therefore, the conversion from  $4.6PF_6$  to  $3.4PF_6$  was tested by refluxing  $4.6PF_6$  in dry MeCN and in the presence of  $\sim$ 5 mol%  $^tBu_4NI$ , followed by the addition of excess  $NH_4PF_6$  in order to effect complete counterion exchange. After being washed with  $H_2O$  and  $CH_2Cl_2$ , the crude solid was subjected to reverse-phase column chromatography, affording a 9:1 ratio of  $4.6PF_6$  to  $3.4PF_6$ . The conversion of  $4.6PF_6$  to  $3.4PF_6$  implies that  $3.4PF_6$  is the thermodynamic product while  $4.6PF_6$  is the kinetic product in these sets of reactions.

**Crystallographic Studies.** Single crystals of  $3.4\text{PF}_6$ ,  $4.6\text{PF}_6$ ,  $7.4\text{PF}_6$ , and  $8.6\text{PF}_6$  were grown by vapor diffusion of  $^i\text{Pr}_2\text{O}$  into a MeCN solution for 3-4 days. Single crystal X-ray studies of different complexes of all the cyclophanes were undertaken to reveal the relationship between the structures of the cyclophanes and their packing in the crystalline state. The presence of a more  $\pi$ -extended polyaromatic unit, such as naphthalene, has a significant influence on the overall packing of these macrocycles. In addition, the local  $C_{2\nu}$  symmetry of the 2,7-disubstituted naphthalene unit allows some degree of

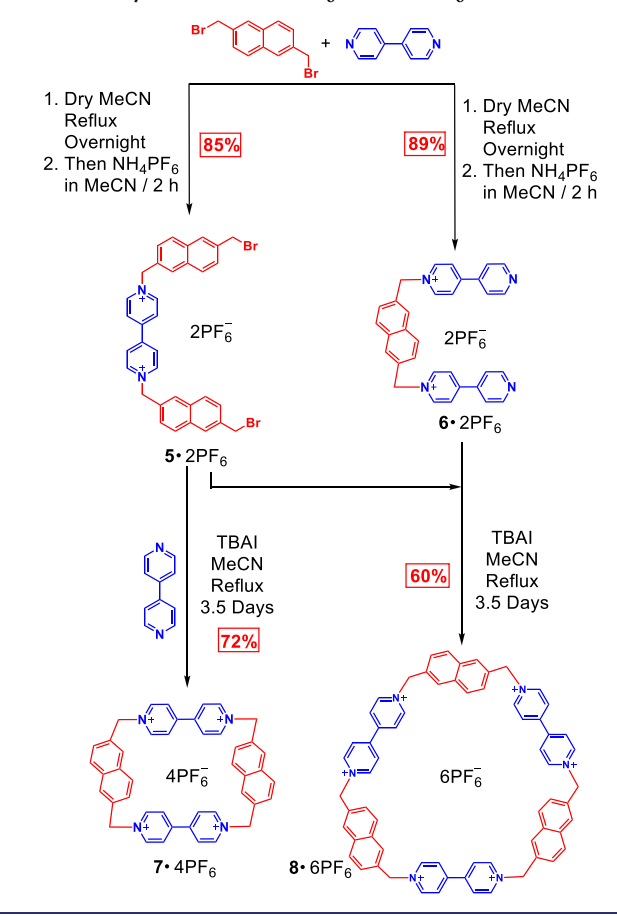
Scheme 1. Syntheses of 3.4PF6 and 4.6PF6



rotational freedom, which results in crystallization of 3.4PF6 into two conformational polymorphic structures, namely  $\alpha$ -3· 4PF<sub>6</sub> and  $\beta$ -3·4PF<sub>6</sub>. As a result of the rotation of the naphthalene units, these structures do not form 2D D-A tiling patterns. See Supporting Information for details, Figures S21 and S22. Reduction of 4.6PF 6 to 4.3PF6 induces a dramatic conformational change in the molecular structure, and the radical-radical pairing interactions (see Figures 3 and S26) between the viologen units becomes superstructure-directing. Detailed structural analysis of 3.4PF<sub>6</sub> and 4.3PF<sub>6</sub> can be found in Supporting Information, while the discussion relating to the structures 4.6PF<sub>6</sub>, 7.PF<sub>6</sub>, and 8.4PF<sub>6</sub> can be found below. On the other hand, co-crystallization of these cyclophanes with a strong donor, such as TTF, in addition to the formation of host-guest D-A complexes, the TTF-viologen CT interactions compete with the intermolecular naphthaleneviologen interactions, leading to changes both in the molecular structures of cyclophanes and in their overall packing in the crystal superstructures. A summary of the crystallographic data for all the compounds is reported in Tables S1-S3.

Crystal Structure of  $4.6PF_6$ .  $4.6PF_6$  crystallizes in the triclinic  $P\overline{1}$  space group with one molecule in the asymmetric unit. The dimensions (Figure 2a) of the cavity calculated from the distance between the naphthalene and the viologen units are approximately (Table S2)  $10 \times 11 \times 12$  Å, resulting in a truncated hexagon-like structure. The angles within the macrocycle lie in the range of  $110-116^\circ$  (mean,  $112^\circ$ ). The  $C_{2\nu}$  point group symmetry of the 2,7-disubstituted naphthalene units allows different geometrical orientations, as observed in the two polymorphs,  $\alpha$ - and  $\beta$ - $3^{4+}$  (Figures 2b, S21, and S22),

Scheme 2. Syntheses of 7.4PF<sub>6</sub> and 8.6PF<sub>6</sub>



and the tris-radical 43(++) (Figure S26) which generate a polygon. The macrocycles interact through face-to-face D-A  $[\pi \cdots \pi]$  interactions in the *ab*-plane between the naphthalene and the viologen units, with interplanar distances of  $\sim 3.5$  Å, to form a hexagonal superstructure (hex-4<sup>6+</sup>) with a confined cavity (Figure 2c) having a diameter of approximately 12 Å. These hex·46+ superstructures tile (Figures 2e and S24a) by means of a set of D-A interactions in a 2D network, and the ATs in 4<sup>6+</sup> can be considered as a case of periodic isogonal tiling by non-edge-to-edge convex regular polygons ( $hex \cdot 4^{6+}$ ) following AT principles. Recent investigations have reported<sup>26</sup> the hexagonal tiling of hexagonal macrocycles of different sizes through a combination of hydrogen bonding and van der Waals interactions to form periodically ordered 2D networks at the liquid-solid interface. Along the c-axis, the macrocycles stack (Figure 2d) in 1D to form molecular channels. The twist angles  $(\theta_1)$  between the pyridinium units (Table S2) of each viologen are 6.4, 20, and 25°. The density functional theory (DFT)-optimized structure exhibits (Figure S38) larger twist angles  $(\theta_1)$  with an average of 42°, which indicates that face-toface D-A interactions between the naphthalene and the bipyridinium units induce planarity in the viologens. A strategy proposed<sup>19</sup> to obtain dual pores in COFs involves desymmetrization of a highly symmetric vertex by elongation of one or more arms of the COF to create non-equilateral polygons. Similarly, in our systems, the supramolecular arrangement of truncated hexagons, through a network of D-A  $[\pi \cdots \pi]$ interactions, generates a 2D material with heterogeneous channels in the crystal structure. One-electron reduction of each viologen unit of 4.6PF6 results in the formation of the

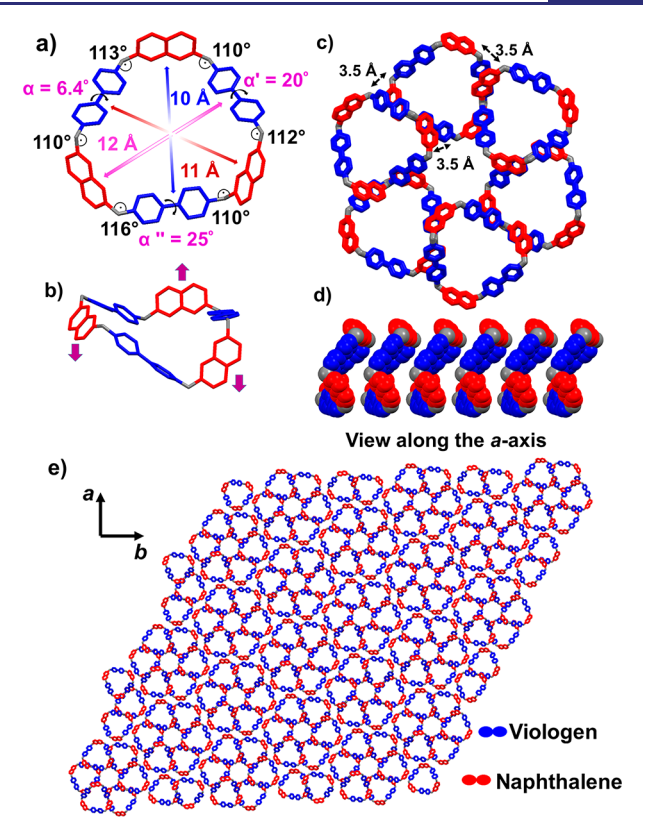


**Figure 2.** Crystal structure of  $4^{6+}(PF_6)$  anions are omitted for the sake of clarity) showing (a) the front view of the asymmetric unit, (b) side view of the asymmetric unit showing a different orientation of the naphthalene units, (c) self-assembly of the  $4^{6+}$  macrocycles through viologen-naphthalene D-A interactions to form a supramolecular hexagonal superstructure  $hex-4^{6+}$ , (d) stack of  $4^{6+}$  to form a tubular superstructure, viewed along the c-axis, and (e) hexagonal tiling of the  $hex-4^{6+}$  through D-A CT interactions in the ab-plane with the P6m symmetry in the Archimedean hexagonal tiling pattern.

tris-radical 4·3PF<sub>6</sub>. All the viologen radical cations adopt a planar conformation (Figures 3 and S26) with inter-ring bipyridinium torsional angles (Table S2) of <6.0°, and the bond length between the pyridinyl groups decreases from 1.48 Å in the dicationic form to 1.42 Å in the radical cation form. All the viologen units dimerize through short  $[\pi^* \cdots \pi^*]$ interactions of  $\leq 3.2$  Å, which is lower than the van der Waals radius of 3.4 Å, to form diamagnetic dimers. These pairs interact through the third viologen unit (Figure 3) which establishes face-to-face  $[\pi^*\cdots\pi^*]$  interactions with viologens symmetrically equivalent to those in an adjacent macrocycle in the bc-plane. In addition, the strong tendency of the viologens to dimerize indicates that the naphthalene-viologen D-A interaction is weaker than that in the viologen radical dimers. Consequently, the naphthalene units are forced to interact through weak face-to-face  $[\pi \cdots \pi]$  interactions (Figure S27) of 3.4 and 3.6 Å along one dimension. Remarkably, the flexible nature of 4.3PF<sub>6</sub> combined with its tendency to form pairs of cyclophanes prevents the formation of a 2D network of polygons. Such behavior potentially can be prevented by using more rigid cyclophanes.

Crystal Structure of **8**·6PF<sub>6</sub>. **8**·6PF<sub>6</sub> crystallizes in the monoclinic C2/c space group with one molecule (Table S1) in the asymmetric unit. The local  $D_{2h}$  symmetry of the 2,6-disubstituted naphthalene unit results in a flat and symmetrical truncated hexagon-like structure with  $D_{3h}$  point group

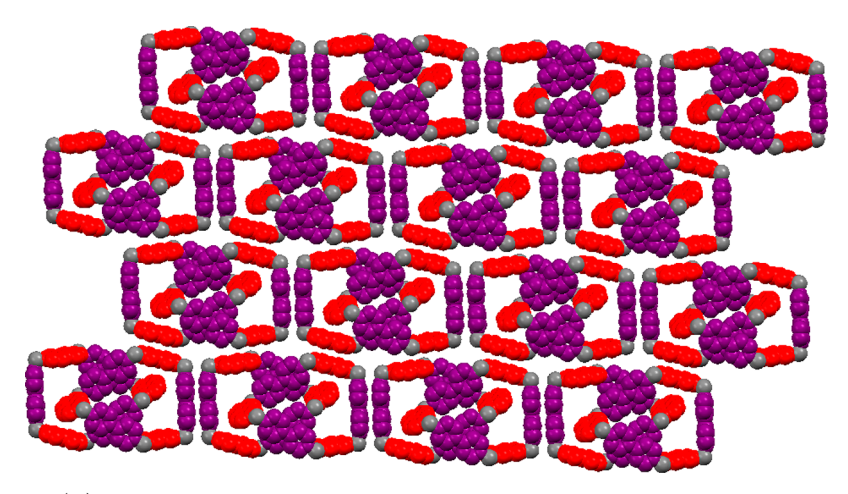


Figure 3. Crystal structure of  $4^{3(\bullet+)}$  showing the propagation of  $[\pi^*\cdots\pi^*]$  interactions between the supramolecular dimers  $(4^{3(\bullet+)})_2$  along one direction to form supramolecular chains. These chains interact through  $[\pi\cdots\pi]$  contacts between the naphthalene units. Viologen radical cations are indicated in purple, naphthalenes in red, and methylene units in gray.

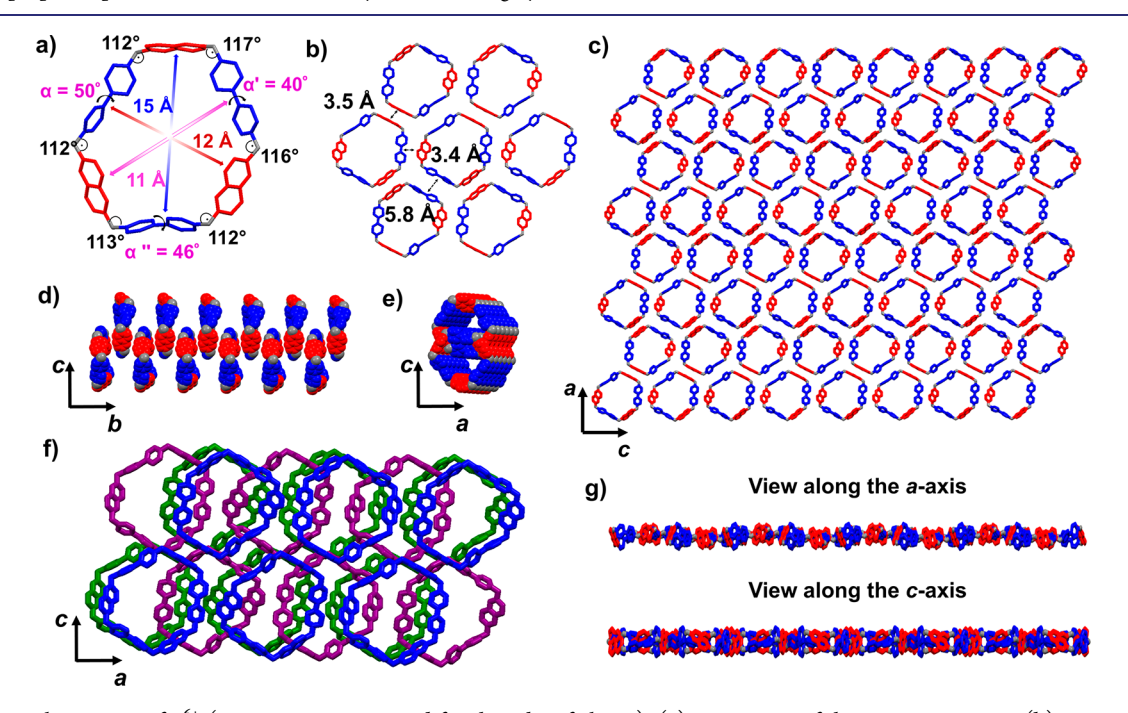


Figure 4. Crystal structure of  $8^{6+}$  (PF<sub>6</sub> anions are omitted for the sake of clarity). (a) Front view of the asymmetric unit. (b) Propagation of the naphthalene—naphthalene [ $\pi \cdots \pi$ ] interactions and naphthalene—viologen D···A interactions in the *ac*-plane. (c) 2D honeycomb hexagonal tiling of  $P_6m$  Euclidean plane symmetry of truncated hexagonal molecular structures. (d, e) Stacking of the macrocycle along the *b*-axis without forming supramolecular channels. (f) View of three layers stacking along the *b*-axis displayed using different colors. (g) Side-view of the layer-like superstructure viewed along the *a*- and *c*-axes.

symmetry. The dimensions of the cavity calculated from the distances between the naphthalene and the viologen units (Figure 4a) are approximately  $11 \times 12 \times 15$  Å, forming a truncated hexagon-like structure with a cavity slightly larger than that of  $4.6\mathrm{PF}_6$ . The angles (Table S2) within the macrocycle ( $\theta_2$ ) are in the range of  $112-117^\circ$  (mean,  $114^\circ$ ). The twist angles ( $\theta_1$ ) between the pyridinium units of each viologen ( $\theta_1$ ) are 40, 46, and 50°. In contrast to the structures of  $3.4\mathrm{PF}_6$ ,  $4.6\mathrm{PF}_6$ , and  $7.4\mathrm{PF}_6$ , where the interplanar interactions lead to a decrease in  $\theta_1$  in the solid state, in the case of  $8.6\mathrm{PF}_6$ , the angles  $\theta_1$  (Table S2) calculated from the crystal structure and gas-phase DFT-optimized structure of  $8^{6+}$  are in the same range. This behavior is the result of the absence of interplanar interactions between the naphthalene and the

viologen units in  $8^{6+}$ ; only weak edge-to-face  $[\pi \cdots \pi]$  interactions exist between the naphthalene and the viologen units, generating a solid-state layer-like structure (Figure 4b) in the ac-plane. Notably, the propagation of the D-A interactions (Figure S25b) are unidirectional along the a-axis, while the face-to-face  $[\pi \cdots \pi]$  interactions (Figure S25a) between the naphthalene units propagate along the c-axis. The hexagonal molecular shape of  $8^{6+}$  self-assembles (Figures 4c and S25c) in a hexagonal manner to form a honeycomb tessellated pattern with P6m symmetry, following the Archimedean tiling principles. Therefore, by contrast with 4-6PF $_6$ , which forms a dual pore superstructure, it is remarkable that the high symmetry of  $8^{6+}$  results in a unipore superstructure. These layer-like superstructures interact with each other through

edge-to-face interactions between the viologen and the naphthalene units (Figure 4f), resulting in tangling of the cyclophanes on each other and forming a non-tubular superstructure.

**Charge-Transfer Complexes with TTF.** The search for a relationship between the molecular structure of the D-A cyclophanes and its effect on the overall packing of the D-A stacks with respect to the electronic properties led to an investigation of the crystal packing of cyclophanes 3.4PF<sub>6</sub>, 4. 6PF6, and 7.4PF6 with an additional donor molecule such as TTF. TTF is a stronger donor than naphthalene, and so the TTF-viologen D-A interactions will become superstructuredirecting, forming a 2D tiling pattern. Furthermore, previous studies<sup>36</sup> revealed that, while tetracationic cyclobis(paraquat-pphenylene) (CBPQT4+) binds a TTF molecule strongly inside its cavity, the molecular square (MS4+) binds two TTF molecules to form a 2:1 complex [2TTFCMS]<sup>4+</sup> or involves a single guest in which the two aromatic planes are inherently stacked together. The nature of the binding was unclear in some cases, as the guest sits at the center of the cavity with equidistant spacing to the viologen units, while in other cases the guest forms a distorted superstructure in which the TTF is displaced from the center of the cavity. To construct CT complexes exhibiting propagation of the CT interactions in 1D and 2D and reveal the effect of the molecular shape of the cyclophane on the overall packing of the D-A complexes, crystallographic studies have been undertaken on all the complexes, and relevant CT salts have been prepared. Cocrystallization of the cyclophanes 3.4PF<sub>6</sub>, 4.6PF<sub>6</sub>, and 7.4PF<sub>6</sub> with an excess of TTF through slow evaporation of the solvent resulted in the formation of green crystals that were suitable for single crystal X-ray diffraction. Several attempts to cocrystallize 8.6PF6 with TTF have been proven to be unsuccessful. The donor-to-acceptor ratios of the resulting complexes were found to be 4:1 in the [3.TTF].4PF6 complex, 7.5:1 in the  $[4 \cdot TTF] \cdot 6PF_6$  complex, and 1:1 in the  $[7 \cdot TTF] \cdot$ 4PF<sub>6</sub> complex. Details of the crystal structures of [3·TTF]· 4PF<sub>6</sub>, [4·TTF]·6PF<sub>6</sub>, and [7·TTF]·4PF<sub>6</sub> are discussed below. The crystallographic data for all the complexes is reported in Table S3.

Crystal Structure of  $[3 \cdot TTF] \cdot 4PF_6$ . The co-crystal  $[3 \cdot TTF] \cdot$  $4PF_6$  crystallizes in the monoclinic space group  $P2_1/c$  with one 3.4PF<sub>6</sub> molecule and four TTF molecules in the asymmetric unit. It is noteworthy that the inclusion of a guest inside the cavity of 34+ allows a change in the orientation of the naphthalene groups to generate larger lengths between the aromatic rings (12 Å), while the width slightly decreases from 7.7 Å in 3.4PF<sub>6</sub> to 7.5 Å in [3.TTF].4PF<sub>6</sub> owing to the relatively strong interactions between the viologen units and the TTF molecules. Nuclear magnetic resonance (NMR) titration (Figure S45) resulted in a relatively small binding constant of  $53 \pm 1 \text{ M}^{-1}$ . For CBPQT<sup>4+</sup>, upon the inclusion of a TTF guest in the cavity, the distance between the viologen units increases from 6.1 to 7.0 Å, resulting in a strong binding constant (Figure S43) of 11 345  $\pm$  1066  $M^{-1}$ . Along the *c*-axis (Figure 5a), two TTF molecules (TTF1 and TTF2) and viologen units form mixed D-A  $\pi$ -stacks with four different interplanar distances. Peierls $^{37}$  pointed out that the instability of 1D metals is pertinent to the distortions that open a gap at the Fermi energy. TTF⊂3·4PF<sub>6</sub> is not centered inside the cavity, with interplanar distances (Figure 5a) from each viologen unit of 3.7 and 3.8 Å. On the other hand, the TTF2 along the  $\pi$ -stack structure interacts with the two viologen

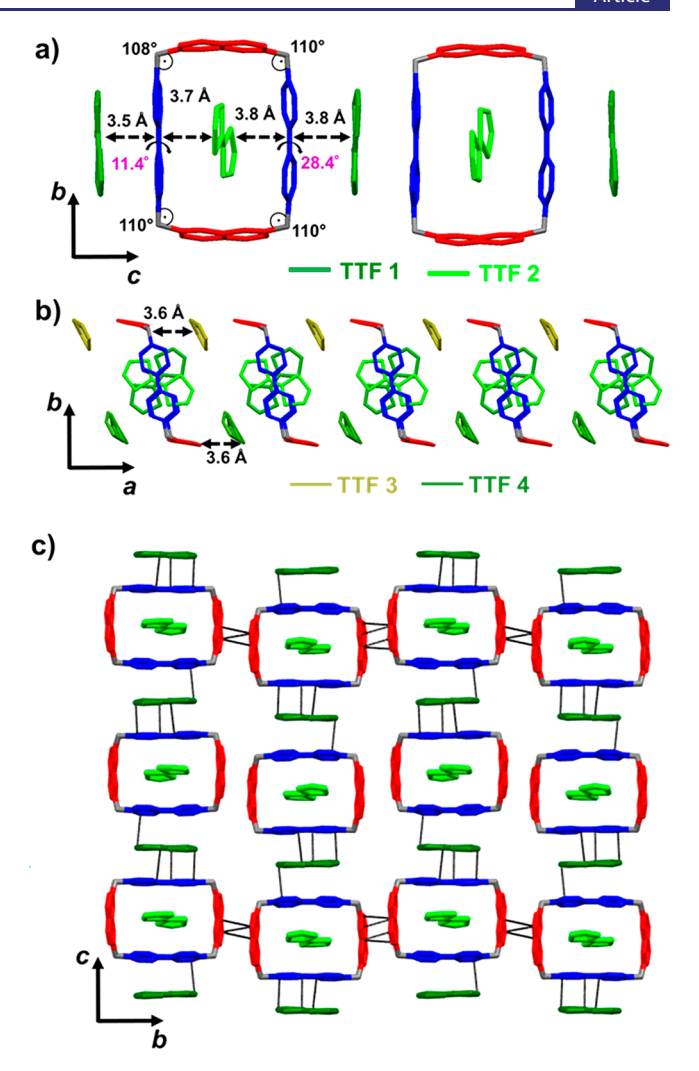


**Figure 5.** Crystal structure of [3·TTF]<sup>4+</sup> (PF<sub>6</sub> anions are omitted for the sake of clarity). (a) Mixed  $\pi$ -stack superstructure propagating along the a-axis and showing distances between the TTF molecules (TTF1 in darker green and TTF2 in bright green) and the viologen units. (b) D-A  $\pi$ -stack between the naphthalene units and TTF molecules (TTF3 in yellow and TTF4 in green) along the a-axis. (c) Tessellation in a cb-plane of the rectangular cyclophanes though TTF–viologen CT interactions and naphthalene–naphthalene [ $\pi$ ··· $\pi$ ] interactions.

units adjacent to the cyclophane with interplanar distances (Figure 5a) of 3.5 and 3.8 Å. Therefore, the D-A  $\pi$ -stack structure of four different alternating intermolecular contacts makes it difficult to predict the electronic properties with respect to the Peierls distortion. In addition, the Peierls distortion of a D-A  $\pi$ -stack at low temperature (100 K) results in the non-central location of TTF within the cavity of  $3.4PF_6$ .

The crystal structure reveals the existence of two other TTF molecules (TTF3 and TTF4) (Figures 5b and S28a) that interact with the naphthalene units through [C-H··· $\pi$ (TTF)] along the a-axis, having contacts of 2.7–3.0 Å and affording another mixed D-A  $\pi$ -stack superstructure. This 2D topology, where two mixed D-A  $\pi$ -stacks coexist in two dimensions, is unique and potentially can exhibit conductive properties in 2D. According to a previous report on CT complexes, <sup>38</sup> the valency of organic molecules, as well as the electron-transporting properties of the materials, can be predicted by analyzing the details of their structures, such as the bond lengths, bond

angles, separation distances, and the packing motifs of donor and acceptor species. In Figure S28, the side view shows that TTF1 and TTF2 are planar, while TTF3 and TTF4 are slightly curved. The structure factors of TTF3 and TTF4 revealed that the S atoms and C atoms of the central C=C double bond are co-planar, while the five-membered rings are bent and lie at a torsion angle of ~16-17°. Such distortion could be a result of weak attractive intermolecular interactions. DFT calculations revealed that the structure of an isolated TTF molecule in the gas phase is not planar. Instead, it adopts a boatlike conformation with a  $C_{2\nu}$  point group symmetry, where the two pentagonal rings are slightly bent with an angle of  $\sim 15^{\circ}$ . In addition, the lengths of the central C=C double bonds of TTF molecules were also examined, as these bond lengths are benchmarks for predicting the oxidation states of TTF species. Because they are adjacent to viologen units, the TTF1 and TTF2 molecules were expected to possess a positive charge, and the central C=C bond was expected to be elongated by the single-bond component from the resonance structure compared to that in the neutral form (TTF3 and TTF4). The C=C bond lengths of TTF1 and TTF2 are 1.33(1) and 1.37(1) Å, respectively, while TTF3 and TTF4 have central C=C bond lengths of 1.33(1) and 1.31(1) Å, respectively. The C=C bond length in neutral TTF was determined to be 1.337 Å, while that in TTF-TCNQ (tetracyanoquinodimethane) is 1.369 Å ( $\rho_{\rm TTF}$  = +0.59).<sup>40</sup> In this context, it is obvious that three TTF molecules (TTF1, TTF3, and TTF4) are in the neutral form, while the fourth one (TTF2) undergoes partial oxidation. It is, however, remarkable that the TTF molecules inside the cavity of the cyclophane are in the neutral form and are slightly more distant from the viologen unit, while the TTFs with shorter distances to the viologen undergo more significant electron transfer. The discrepancy in the twist angles  $(\theta_1)$  of the two viologen units (11 and 28°) indicates that, while the planar viologen is in a partially reduced form, the second viologen is still in its dicationic oxidation state. Electron paramagnetic resonance (EPR) studies (Figure S37) of [3·TTF]·4PF<sub>6</sub> in the solid state revealed the existence of an anisotropic signal with  $g_{\rm iso} = 2.006$  characteristic of TTF<sup>•+</sup>.

Crystal Structures of 7.4PF<sub>6</sub> and [7.TTF].4PF<sub>6</sub>. The crystal structure of macrocycle 7.4PF6 revealed that it crystallizes in the triclinic P1 space group with two symmetrically distinct half-cyclophanes (Figure S24a) in the asymmetric unit. In contrast to the 2,7-naphthalene units, which possess some rotational flexibility, the local  $D_{2h}$  symmetry of the 2,6naphthalene units are structurally more rigid within the structures of cyclophanes. The angles of the macrocycles on the methylene corners are 107-109° (Figure S24b) and are slightly smaller than those of 3.4PF<sub>6</sub>, but similar to those of CBQPT <sup>4+</sup>. The twist angles  $(\theta_1)$  between the pyridinium rings of the viologens are 18 and 31° (Figure S24b), which are slightly larger than those of 3.4PF<sub>6</sub>. The DFT-optimized structure shows a larger twist angle  $(\theta_1)$  of 41°, which confirms once again that the face-to-face D-A interactions between the naphthalene and the viologen units induce a slight decrease in the twist angle  $(\theta_1)$  of the viologen units (Table S2). The dimensions of the cavity, estimated from the distances between the aromatic planes on opposite sides of the empty cyclophane in the X-ray crystal structure (Figure S24b), were 9.1 Å (width) and 10 Å (length) or approximately 5.7 Å (width)  $\times$ 6.9 Å (length) when considering the van der Waals radii. Both the width and the length of 7<sup>4+</sup> are larger than those of 3<sup>4+</sup> but

smaller than those of a tetracationic molecular square (MS<sup>4+</sup>), cyclobis(paraquat-4,4'-biphenylene). The arrangement of 7. 4PF 6 in the crystal structure is similar to that of CBPQT<sup>4+</sup>,

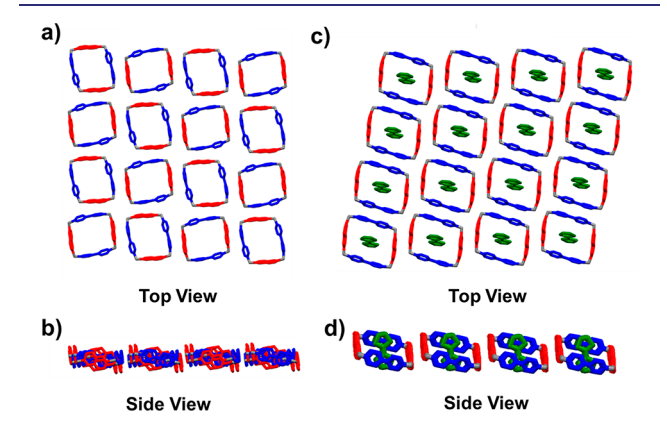


Figure 6. Crystal structure of 7<sup>4+</sup> showing (a) the top view of tiled cyclophanes through 2D D-A interactions and (b) the side view of the layer-like superstructure. Crystal structure of [7·TTF]<sup>4+</sup> showing (c) the top view of TTFC  $7^{4+}$  tiling through naphthalene—naphthalene  $[\pi \cdots \pi]$  interactions and (d) the side view of the propagation of  $[\pi \cdots \pi]$ interactions between the naphthalene units propagating along one direction. PF6 anions are omitted for the sake of clarity.

where the naphthalene and viologen units interact in a face-toface manner with interplanar distances in the range of 3.3–3.6 Å (Figure 6a,b). These supramolecular D-A interactions propagate in the cb-plane to form tessellation patterns of two symmetrically distinct polygons (Figure S24c) similar to the Archimedean tiling of squares. Stacking of these 2D layers results in 1D molecular square channels (Figure S24d). It is noteworthy that [7·TTF]·4PF<sub>6</sub> does not form a mixed D-A 1D stack but adopts (Figures 6a,b and S32) as well square tessellations in a 2D plan; however, the superstructuredirecting interactions are  $[\pi \cdots \pi]$  naphthalene—naphthalene interactions rather than naphthalene-viologen D-A inter-

Crystal Structure of [4:TTF].6PF<sub>6</sub>. The hexagonal shape of 4<sup>6+</sup> is expected to generate different D-A packing in the solid state. The growth of the 46+. TTF co-crystal was achieved through slow evaporation of solvent due to low affinity of TTF to the cavity of the 4<sup>6+</sup> cyclophane (see <sup>1</sup>H NMR titration Figure S47). The co-crystal [4.TTF]-6PF<sub>6</sub> crystallizes (Figure 7a) in the monoclinic  $P2_1/n$  space group with one cyclophane molecule and 7.5 TTF molecules in the asymmetric unit. Seemingly, the co-crystals of both  $[3 \cdot TTF] \cdot 4PF_6$  and  $[4 \cdot TTF] \cdot$ 6PF<sub>6</sub> crystallize in higher symmetry compared to 3·4PF<sub>6</sub> and 4· 6PF<sub>6</sub>. Five TTF (Type I and Type II) molecules among the total number of TTFs in the asymmetric unit are involved (Figure 7a) in the D-A face-to-face interactions with the viologen units. The interplanar distances between the TTF molecules and the viologen units are in the range of 3.3–3.5 Å. These distances are adequate for charge transfer, and some of them are shorter than those of [3·TTF]·4PF<sub>6</sub>. These D-A CT interactions (Figure 8b,d) propagate in a hexagonal manner in the ab-plane. The hexagon-like superstructure of six assembled cyclophanes and TTFs in the ab-plane is interconnected through naphthalene–naphthalene  $[\pi \cdots \pi]$  interactions (Figure 8a,c) of  $\sim 3.4$  Å of another cyclophane. These  $[\pi \cdots \pi]$ interactions between naphthalene units propagate also in a 2D layer to form a hexagonal tessellation pattern. It is

Journal of the American Chemical Society

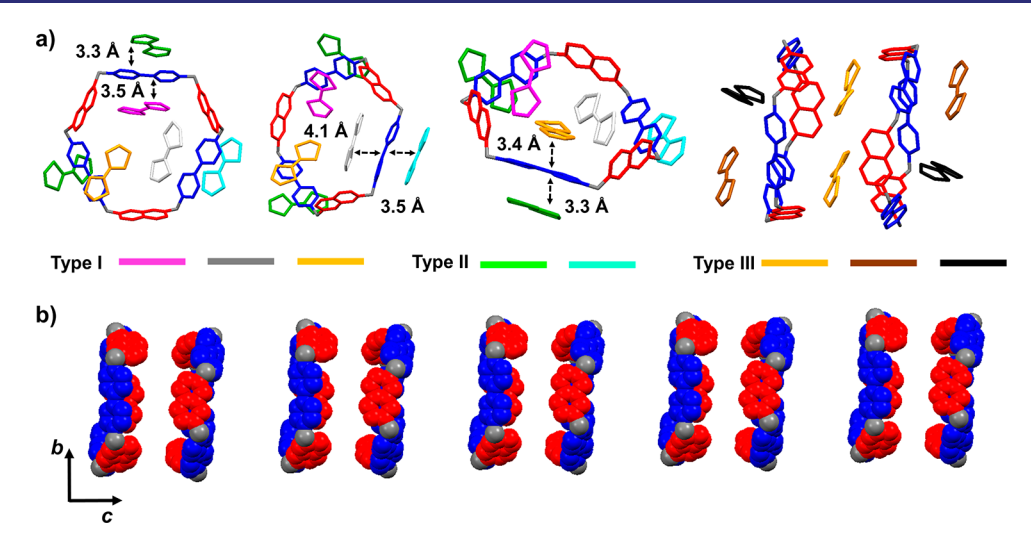


Figure 7. Crystal structure and superstructure of  $[4 \cdot TTF]^{6+}$  (PF<sub>6</sub> anions are omitted for the sake of clarity). (a) D-A interaction of each viologen unit with two TTF molecules (Type I, inside the cavity, and Type II, around the cyclophane), and non-π-stacking TTF molecules (Type III). (b) Arrangement of the polygons along the *c*-axis to form supramolecular channels.

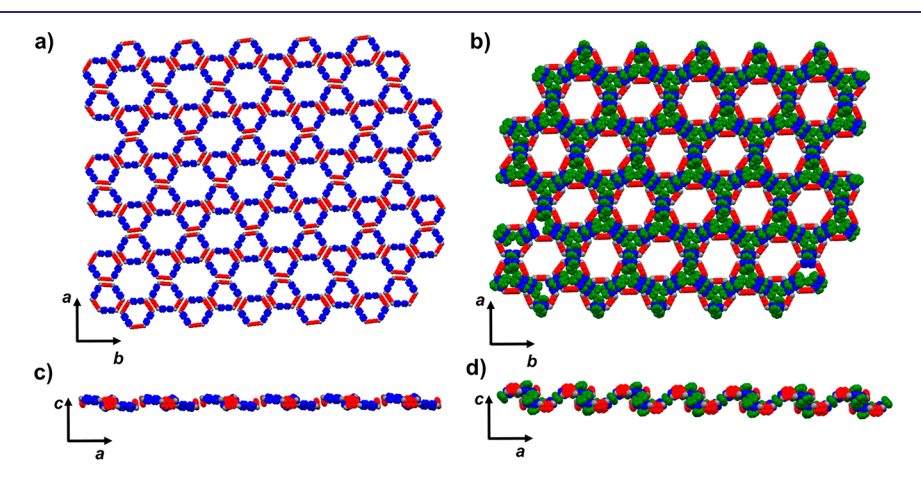


Figure 8. Crystal structure and superstructure of  $[4 \cdot TTF]^{6+}$  (PF<sub>6</sub> anions are omitted for the sake of clarity). (a) Hexagonal tiling of the cyclophanes through naphthalene—naphthalene  $[\pi \cdots \pi]$  interactions. (b) Hexagonal tiling of the cyclophanes through CT interactions between TTF and viologen. The three TTF molecules inside the macrocycle form a TTF triad through close  $[S \cdots S]$  contacts. (c, d) Side views of thelayer-like superstructures.

remarkable that the co-crystallization of 4.6PF<sub>6</sub> with TTF changes the 2D network from the heterogeneous pores in 4· 6PF<sub>6</sub> to the regular honeycomb Archimedean tiling in the [4· TTF]-6PF<sub>6</sub> co-crystal. Among the Type I and II TTFs, three of them and two viologen units exhibit rotation angles (Figure S30) in the range of  $49-72^{\circ}$ , while the third viologen and two others are nearly parallel, with a rotation angle of 10°. Three other TTF molecules (Type III) are not involved (Figure 7a) in the interplanar D-A interactions. One of these Type III TTF molecules interacts in an edge-to-face manner with the naphthalene unit (2.7 Å), while the other TTF establishes several [S···S] and hydrogen-bonding interactions with adjacent TTF molecules. Structure factors of Type III TTF molecules revealed that the S atoms and C atoms of the central C=C double bond are coplanar, while the five-membered rings are bent along the dithiol line with torsion angles of  $\sim 14$ and 18°. The thermal disorder of the TTF units hampers detailed analysis of their oxidation state through analysis of the C=C bond length. Therefore, analysis of the viologen units, which are structurally well-defined, can give some information about the oxidation state of the cyclophane and TTFs. The

twist angles  $(\theta_1)$  of the three viologen units (Table S2) are 5.1, 5.9, and 15°, while the C-C bonds between the pyridinium units have lengths of 1.43, 1.44, and 1.46 Å, respectively. Both the distances and the angle values correlate with the distances between the TTF and viologen units, where shorter CT distances result in small twist angles  $(\theta_1)$ . The short C-C distances and small twist angles  $(\theta_1)$  of the pyridinium units of two viologens are indicative of their cation-radical character, while the third viologen is most likely only partially reduced. Indeed, the C-C bond lengths in  $3.4PF_6$  are  $\sim 1.48$  Å, while those in the tris-radical 4.3PF<sub>6</sub> are around 1.43 Å. It is noteworthy that the three TTF molecules in the cavity of the macrocycle are in close contact with each other, with distances in the range of 2.7–3.5 Å, forming a unique TTF-triad (Figure 7) that provides an potential additional pathway for electron transfer between the mixed D-A stacks in addition to the intramolecular CT in the cyclophane (vide infra). Previous studies<sup>36</sup> reported the stabilization of  $(TTF_2)^{\bullet+}$  and  $(TTF^{\bullet+})_2$ radicals in the viologen cyclophane CPBQT4+ through interlocked catenanes. We recently reported<sup>34</sup> that the tessellatessellation of NDI- $\Delta$  and TTF leads to the formation of twodimensional hexagonal patterns containing two different triangles, namely NDI- $\Delta$  and TTF- $\Delta$ . We demonstrated that utilization of non-planar geometries can lead to inhibition of the dimerization of  $TTF^{\bullet+}$ , and that supramolecular  $TTF-\Delta$ was determined to have a mixed-valence character between one neutral TTF molecule and two TTF<sup>++</sup> radical cations, with an absorption in the mid IR ( $\lambda_{max}$  = 2500 nm) range. Similarly, the hexagonal geometry of 4<sup>6+</sup> plays a crucial role in preventing the TTF radicals from forming dimers. Similar to the structure of 4.3PF61 in which the radical-radical dimerization (Figure 3c) is the structure-directing interaction, in the  $[4 \cdot TTF] \cdot 6PF_6$ co-crystal the CT interactions between the TTF and the viologen compete with naphthalene-viologen interactions. Therefore, TTF-viologen CT interactions are the structuredirecting interactions that lead to the formation of a tubular superstructure (Figures 7b and S31) with uniform pores. Similar to [3·TTF]·4PF<sub>6</sub>, EPR studies (Figure S37) of [4· TTF]·6PF<sub>6</sub> in the solid state revealed the existence of an anisotropic signal with  $g_{iso} = 2.0053$  characteristic of the TTF<sup>•+</sup>. Absorption spectroscopy of a thin film of [4·TTF]· 6PF<sub>6</sub> confirmed the existence of CT from TTF to the viologen

Solution Absorption and Fluorescence Studies. The association of the naphthalene and viologen moieties within a macrocycle can induce a twisted intramolecular charge transfer (TICT) that may influence charge transport through the networks. Steady-state absorption and fluorescence studies have been undertaken on the cyclophanes  $3\cdot4\mathrm{PF}_{6}$ ,  $4\cdot6\mathrm{PF}_{6}$ ,  $7\cdot4\mathrm{PF}_{6}$ , and  $8\cdot6\mathrm{PF}_{6}$  in solution. The absorption and fluorescence spectra were measured in very dilute solutions (<10<sup>-5</sup> M) to avoid aggregation. The results are summarized in Table S4.

All the absorption spectra of the four different cyclophanes exhibit two intense absorption peaks at ~230 and 265 nm (Figure 9), which are characteristic of the  $[\pi \rightarrow \pi^*]$  transitions for the naphthalene and viologen units, respectively. However, a weak band at ~465 nm with a molar absorption coefficient in the range of 7100–8460  $M^{-1}$ ·cm<sup>-1</sup> is observed and attributed to the intramolecular CT from the naphthalene to the viologen unit. This transition extends to lower wavelengths, appearing as a shoulder on the strong 265 nm transition. DFT calculations using the B3LYP functional<sup>42</sup> and 6-31G\*\* basis set (Table S5 and Figures S38-S41) revealed that the highest occupied molecular orbital (HOMO) is localized on the naphthalene moiety, while the lowest unoccupied molecular orbital (LUMO) is localized on the viologen unit with an energy difference of ~2.10 eV, which supports the assignment of this transition having CT character. Likewise, dicationic dimethyl viologen (MV<sup>2+</sup>) does not show this transition at 465 nm.

Upon excitation of the  $[\pi \to \pi^*]$  transitions of  $MV^{2+}$  in acetonitrile at 265 nm, the emission (Figure S33) shows a maximum at 355 nm with a Stokes shift of 9600 cm<sup>-1</sup>. The fluorescence lifetime is  $1.00 \pm 0.04$  ns, with a quantum yield of  $0.03 \pm 0.01$ .<sup>43</sup> By contrast, fluorescence studies (Table S4 and Figures 10 and S34) of cyclophanes  $3^{4+}$ ,  $4^{6+}$ ,  $7^{4+}$ , and  $8^{6+}$  revealed no similar emission upon excitation at 265 nm, but instead showed a weak emission in the green region at 540 nm. On the other hand, excitation of the CT band at 465 nm results in a more intense green emission at 540 nm with fluorescence quantum yields of  $1.3 \pm 0.1\%$ ,  $2.3 \pm 0.2\%$ , and  $4.0 \pm 0.5\%$  for  $3^{4+}$ ,  $7^{4+}$ , and  $8^{6+}$ , respectively. The emissive band at 540 nm likely owes its origin to radiative recombination of this CT state, which may undergo structural relaxation between conformers prior to recombination. The stokes shift between

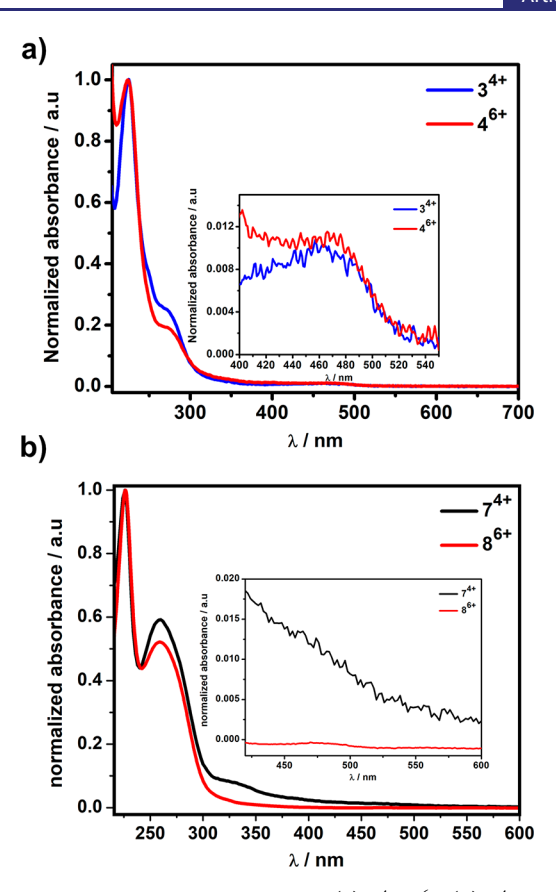


Figure 9. UV–vis absorption spectra of (a)  $3^{4+}$ ,  $4^{6+}$ , (b)  $7^{4+}$ , and  $8^{6+}$  in MeCN.

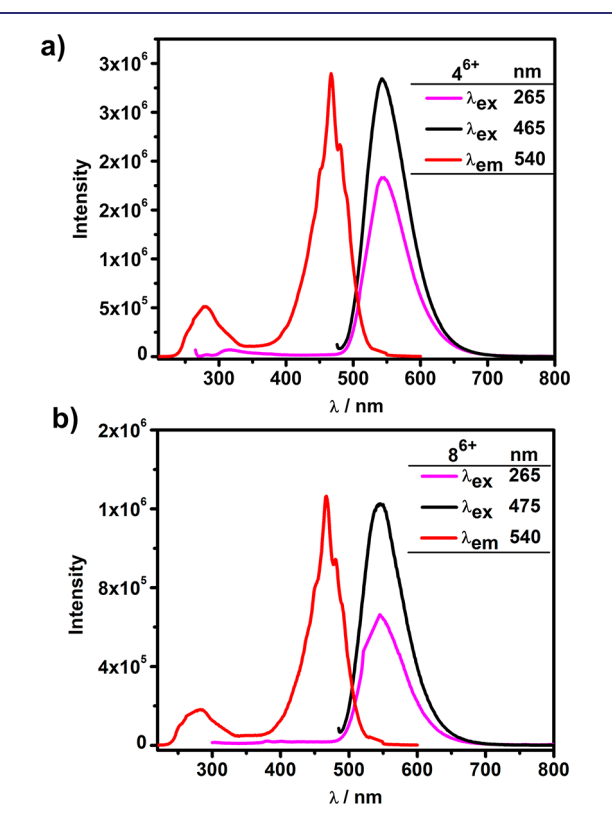


Figure 10. Excitation and emission spectra of  $4^{6+}$  (a) and  $8^{6+}$  (b) in MeCN

the fluorescence excitation at 465 nm and the emission at 540 nm is ca. 3000 cm<sup>-1</sup>, which further supports a structural or solvent rearrangement following excitation.<sup>46</sup>

Previous studies<sup>45</sup> have shown that the conformational constraints on viologen derivatives induced by a host enhance the viologen-based emission. More recent studies<sup>44</sup> have shown that viologen-tetraarylborate ion-pair complexes possess a CT transition at 370 nm leading to the formation of the viologen radical, which undergoes structural changes in the excited state. Here, the naphthalene serves as the electrondonating unit, held at a close distance to the viologen, though with different orientations between the different macrocycles, and its interaction with the viologen unit leads to the CT band in the absorption spectrum. Recent studies<sup>44</sup> have shown the existence of two predominant conformers in the ground state of MV<sup>2+</sup> with different excited-state dynamics. The two conformers ( $\alpha$  and  $\beta$ ) of viologen depend on the torsion angle of the pyridinium units, and each shows different emission features for the CT state. While the CT state of the  $\alpha$ conformer leads to emission at 520 nm, the  $\beta$  conformer emits at 550 nm; the energy difference between these states is  $\sim$ 1050 cm<sup>-1</sup>, which suggests that the Stokes shift discussed above can be attributed in part to structural changes following excitation. The discrepancy of the photophysical behavior between excitations at 265 and 465 nm may also indicate a change of viologen conformation after excitation in the CT band. The intensity of the 540-nm emission suggests either a strong prevalence of the  $\beta$  conformer in the ground state or rapid conversion to the  $\beta$  conformer in the excited state.

Indeed, analysis of the fluorescence decay at 540 nm reveals a single component with a lifetime (Table S4) of 2.16-2.93 ns, which suggests that any structural change following excitation is fast. In this context, the efficient intramolecular CT from the naphthalene to the viologen unit induces stabilization of the  $\beta$  conformer, which quenches the emission from the  $\alpha$  conformer completely and results in a unique emission at 540 nm associated with the  $\beta$  conformer. The mechanism and energetics are shown schematically in Figure 11. The observation of TICT in soution-phase polycationic cyclophanes could potentially be exploited in sensors for detecting solvent, (micro)viscosity, and chemical species.

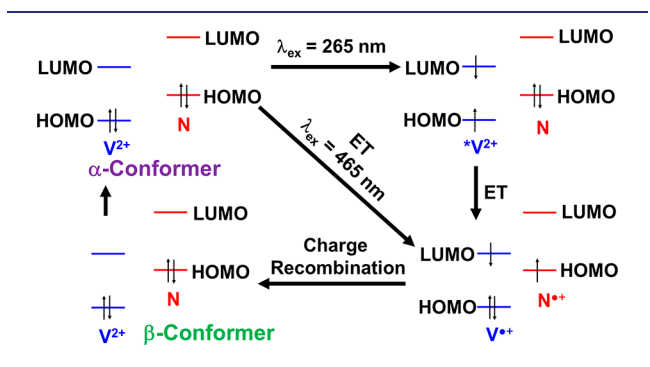
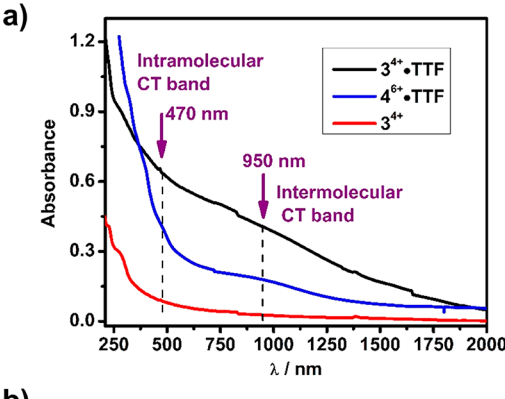


Figure 11. Proposed mechanism for the formation of viologen radical  $(V^{\bullet+})$  at photoexcitations of 265 and 465 nm. N is naphthalene.

**Solid-State Absorption Spectroscopic Studies.** The solid-state optical properties of the polycationic cyclophanes and their co-crystals with TTF molecules have been investigated (Figures 12 and S36) in thin films that are prepared by drop-casting. All the cyclophanes display similar absorption profiles, with very weak CT bands that are centered



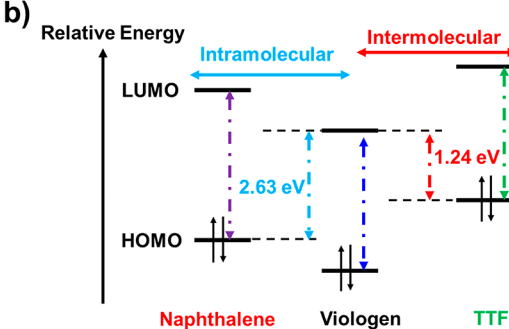


Figure 12. (a) Solid-state UV-vis absorption spectra of 3<sup>4+</sup>, [3·TTF]<sup>4+</sup>, and [4·TTF]<sup>6+</sup>. (b) Schematic energy diagram of the frontier orbitals of the naphthalene, viologen, and TTF.

on 470 nm, resulting from not only intramolecular CT, as observed in solution, but also intermolecular CT between naphthalene and viologen units. The co-crystals of cyclophanes with TTF display rather different optical properties with the emergence of a broad absorption band near the IR region (>700 nm). While the [3·TTF]<sup>4+</sup> is characterized by the presence of an absorption band in the range of 650-2000 nm, the CT complex [4·TTF]6+ has an absorption band in the range of 600-1500 nm, indicative of the lowering of the band gap of the 1D stack compared with that of the hexagonal superstructure [4·TTF]6+. Similarly, the absorption profiles of both [7·TTF]<sup>4+</sup> and [8·TTF]<sup>6+</sup> display bands at ~500 and 1000 nm associated with the intra- and intermolecular CT transfer in naphthalene-viologen and TTF-viologen D-A pairs. In this context, the dual intra- and intermolecular CT in 2D tiling networks can afford additional degrees of freedom for electron transport in multiple dimensions in CT organic materials.

# CONCLUSIONS

A series of intramolecular D-A cyclophanes of different sizes, shapes, and point-group symmetries have been prepared in high yields. In solution, all the cyclophanes reveal the existence of a photoinduced intramolecular CT between the naphthalene (D) and viologen (A) units at 465 nm. This intramolecular CT can occur either in the ground state ( $\lambda_{\rm ex}=465$  nm) or in the excited state ( $\lambda_{\rm ex}=265$  nm) and triggers structural changes in the viologen units to offer a new conformation—the  $\beta$  conformer—which emits at 540 nm. In the solid state, careful control of the shape and symmetry of alternating D and A units in the cyclophanes is a powerful approach for accessing square and hexagonal 2D tiling networks through intermolecular D-A  $[\pi\cdots\pi]$  interactions. The box-like cyclophane forms a square tiling pattern with 2D D-A  $[\pi\cdots\pi]$  interactions, while

the hexagon-like cyclophane adopts a honeycomb 2D tiling pattern through a series of naphthalene—naphthalene  $[\pi \cdots \pi]$ and D-A naphthalene-viologen interactions. The truncated hexagonal structure of the 2,6-disubstituted naphthalene-based cyclophane prefers to adopt a hexagonal tiling through D-A interactions to form a supramolecular hexagon which tiles in a hexagonal fashion. Co-crystallization of the cyclophanes with TTF leads to modifications in the tiling motifs as a result of strongly directing TTF-viologen CT interactions, creating well-ordered superstructures with CT interactions propagating in 1D and 2D in the square and hexagonal cyclophanes, respectively. Absorption spectroscopy performed on the cyclophanes in the solid state revealed the persistence of the intramolecular naphthalene-viologen photoinduced CT at 470 nm, while in the presence of TTF an additional absorption band in the NIR region (~1000 nm) emerges as the result of intermolecular TTF-viologen charge transfer. The coexistence of intra- and intermolecular CT in organic materials, combined with the 2D tessellations based on CT interactions, can facilitate multi-dimensional electron transport. In addition, the dual photoinduced charge transfer at two different excitation wavelengths augurs well for their use in the development of multi-responsive organic electronic and optoelectronic materi-

## ASSOCIATED CONTENT

# Supporting Information

The Supporting Information is available free of charge on the ACS Publications website at DOI: 10.1021/jacs.9b07877.

Experimental details, including synthesis, NMR, and supporting figures; crystallographic details of all the crystal structures; EPR; additional UV/vis absorption studies in solution and in the solid state; electrochemical studies using cyclic voltammetry of all the cyclophanes; and information on the DFT calculations undertaken on  $3^{4+}$ ,  $4^{6+}$ ,  $7^{4+}$ , and  $8^{6+}$ , including Figures S1–S48 and Tables S1–S5 (PDF)

X-ray crystallographic information files (CIFs) for 3·4PF<sub>6</sub>, 4·6PF<sub>6</sub>, 7·4PF<sub>6</sub>, and 8·6PF<sub>6</sub> (ZIP)

#### AUTHOR INFORMATION

# **Corresponding Author**

\*stoddart@northwestern.edu

#### ORCID ®

M. Mustafa Cetin: 0000-0002-6443-0232 Yassine Beldjoudi: 0000-0002-9500-4308 Youn Jue Bae: 0000-0003-4006-2292 Ryan M. Young: 0000-0002-5108-0261 Matthew D. Krzyaniak: 0000-0002-8761-7323 Michael R. Wasielewski: 0000-0003-2920-5440 J. Fraser Stoddart: 0000-0003-3161-3697

## **Author Contributions**

\*M.M.C. and Y.B. contributed equally.

#### Notes

The authors declare no competing financial interest.

## ACKNOWLEDGMENTS

This research is part of the Joint Center of Excellence in Integrated Nano-Systems (JCIN) at King Abdulaziz City of Science and Technology (KACST) and Northwestern University (NU). The authors would like to thank both

KACST and NU for their continued support of this research. This project was also supported by the National Science Foundation under grant number DMR-1710104 (M.R.W.). We thank the personnel in the Integrated Molecular Structure Education and Research Center (IMSERC) at Northwestern University (NU) for their assistance in the collection of the data.

## REFERENCES

- (1) (a) Gomes, K. K.; Mar, W.; Ko, W.; Guinea, F.; Manoharan, H. C. Designer Dirac Fermions and Topological Phases in Molecular Graphene. *Nature* **2012**, 483, 306–310. (b) Xu, M.; Liang, T.; Shi, M.; Chen, H. Graphene-Like Two-Dimensional Materials. *Chem. Rev.* **2013**, 113, 3766–3798. (c) Kambe, T.; Sakamoto, R.; Kusamoto, T.; Pal, T.; Fukui, N.; Hoshiko, K.; Shimojima, T.; Wang, Z.; Hirahara, T.; Ishizaka, K.; Hasegawa, S.; Liu, F.; Nishihara, H. Redox Control and High Conductivity of Nickel Bis(dithiolene) Complex π-Nanosheet: A Potential Organic Two-Dimensional Topological Insulator. *J. Am. Chem. Soc.* **2014**, 136, 14357–14360.
- (2) (a) Jin, Y.; Hu, Y.; Zhang, W. Tessellated Multiparous Two-Dimensional Covalent Organic Frameworks. *Nat. Rev. Chem.* **2017**, *1*, 56. (b) Lange, R. Z.; Hofer, G.; Weber, T.; Schlüter, A. D. A Two-Dimensional Polymer Synthesized through Topochemical [2 + 2]-Cycloaddition on the Multigram Scale. *J. Am. Chem. Soc.* **2017**, *139*, 2053–2059.
- (3) Grabar, A. The Art of The World: Art of The Byzantine Empire; Greystone Press: New York, 1967.
- (4) Grünbaum, B.; Shephard, G. C. Tilings and Patterns; W. H. Freeman & Co.: New York, 1986.
- (5) McMahon, M. I.; Degtyareva, O.; Nelmes, R. J. Ba-IV-Type Incommensurate Crystal Structure in Group-V Metals. *Phys. Rev. Lett.* **2000**, *85*, 4896–4899.
- (6) (a) Schlickum, U.; Decker, R.; Klappenberger, F.; Zoppellaro, G.; Klyatskaya, S.; Auwärter, W.; Neppl, S.; Kern, K.; Brune, H.; Ruben, M.; Barth, J. V. Chiral Kagomé Lattice from Simple Ditopic Molecular Bricks. *J. Am. Chem. Soc.* **2008**, *130*, 11778–11782. (b) Tahara, K.; Furukawa, S.; Uji-i, H.; Uchino, T.; Ichikawa, T.; Zhang, J.; Mamdouh, W.; Sonoda, M.; De Schryver, F. C.; De Feyter, S.; Tobe, Y. Two-Dimensional Porous Molecular Networks of Dehydrobenzo[12]annulene Derivatives via Alkyl Chain Interdigitation. *J. Am. Chem. Soc.* **2006**, *128*, 16613–16625.
- (7) Chen, B.; Zeng, X.; Baumeister, U.; Ungar, G.; Tschierske, C. Liquid Crystalline Networks Composed of Pentagonal, Square, and Triangular Cylinders. *Science* **2005**, *307*, 96–99.
- (8) Takano, A.; Kawashima, W.; Noro, A.; Isono, Y.; Tanaka, N.; Dotera, T.; Matsushita, Y. A Mesoscopic Archimedean Tiling Having a New Complexity in an ABC Star Polymer. *J. Polym. Sci., Part B: Polym. Phys.* **2005**, 43, 2427–2432.
- (9) Talapin, D. V.; Shevchenko, E. V.; Bodnarchuk, M. I.; Ye, X.; Chen, J.; Murray, C. B. Quasicrystalline Order in Self-Assembled Binary Nanoparticle Superlattices. *Nature* **2009**, *461*, 964–967.
- (10) Millan, J. A.; Ortiz, D.; van Anders, G.; Glotzer, S. C. Self-Assembly of Archimedean Tilings with Enthalpically and Entropically Patchy Polygons. *ACS Nano* **2014**, *8*, 2918–2928.
- (11) Ueda, K.; Dotera, T.; Gemma, T. Photonic Band Structure Calculations of Two-Dimensional Archimedean Tiling Patterns. *Phys. Rev. B* **2007**, *75*, 195122.
- (12) Kim, Y.; Han, H.; Kim, Y.; Lee, W.; Alexe, M.; Baik, S.; Kim, J. K. Ultrahigh Density Array of Epitaxial Ferroelectric Nanoislands on Conducting Substrates. *Nano Lett.* **2010**, *10*, 2141–2146.
- (13) Basnarkov, L.; Urumov, V. Diffusion on Archimedean Lattices. *Phys. Rev. E* **2006**, *73*, 046116.
- (14) Côte, A. P.; Benim, A. I.; Ockwig, N. W.; O'Keeffe, M.; Matzger, A. J.; Yaghi, O. M. Porous, Crystalline, Covalent Organic Frameworks. *Science* **2005**, *310*, 1166–1170.
- (15) (a) Doonan, C. J.; Tranchemontagne, D. J.; Glover, T. G.; Hunt, J. R.; Yaghi, O. M. Exceptional Ammonia Uptake by a Covalent Organic Framework. *Nat. Chem.* **2010**, *2*, 235–238. (b) Furukawa,

- H.; Yaghi, O. M. Storage of Hydrogen, Methane, and Carbon Dioxide in Highly Porous Covalent Organic Frameworks for Clean Energy Applications. *J. Am. Chem. Soc.* **2009**, *131*, 8875–8883. (c) Han, S. S.; Furukawa, H.; Yaghi, O. M.; Goddard III, W. A. Covalent Organic Frameworks as Exceptional Hydrogen Storage Materials. *J. Am. Chem. Soc.* **2008**, *130*, 11580–11581.
- (16) (a) Lin, S.; Diercks, C. S.; Zhang, Y.-B.; Kornienko, N.; Nichols, E. M.; Zhao, Y.; Paris, A. R.; Kim, D.; Yang, P.; Yaghi, O. M.; Chang, C. J. Covalent Organic Frameworks Comprising Cobalt Porphyrins for Catalytic CO<sub>2</sub> Reduction in Water. *Science* 2015, 349, 1208–1213. (b) Xu, H.; Gao, J.; Jiang, D. L. Stable, Crystalline, Porous, Covalent Organic Frameworks as a Platform for Chiral Organocatalysts. *Nat. Chem.* 2015, 7, 905–912. (c) Ding, S.-Y.; Gao, J.; Wang, Q.; Zhang, Y.; Song, W.-G.; Su, C.-Y.; Wang, W. Construction of Covalent Organic Framework for Catalysis: Pd/COF-LZU1 in Suzuki-Miyaura Coupling Reaction. *J. Am. Chem. Soc.* 2011, 133, 19816–19822.
- (17) (a) Dogru, M.; Handloser, M.; Auras, F.; Kunz, T.; Medina, D.; Hartschuh, A.; Knochel, P.; Bein, T. A Photoconductive Thienothiophene-Based Covalent Organic Framework Showing Charge Transfer towards Included Fullerene. *Angew. Chem., Int. Ed.* **2013**, *52*, 2920–2924. (b) Colson, J. W.; Woll, A. R.; Mukherjee, A.; Levendorf, M. P.; Spitler, E. L.; Shields, V. B.; Spencer, M. G.; Park, J.; Dichtel, W. R. Oriented 2D Covalent Organic Framework Thin Films on Single-Layer Graphene. *Science* **2011**, *332*, 228–231. (c) Wan, S.; Guo, J.; Kim, J.; Ihee, H.; Jiang, D. L. A Belt-Shaped, Blue Luminescent, and Semiconducting Covalent Organic Framework. *Angew. Chem., Int. Ed.* **2008**, *47*, 8826–8830.
- (18) (a) Ma, H.; Liu, B.; Li, B.; Zhang, L.; Li, Y.-G.; Tan, H.-Q.; Zang, H.-Y.; Zhu, G. Cationic Covalent Organic Frameworks: A Simple Platform of Anionic Exchange for Porosity Tuning and Proton Conduction. *J. Am. Chem. Soc.* **2016**, *138*, 5897–5903. (b) Xu, H.; Jiang, D. L. Covalent Organic Frameworks Crossing the Channel. *Nat. Chem.* **2014**, *6*, 564–566. (c) Chandra, S.; Kundu, T.; Kandambeth, S.; BabaRao, R.; Marathe, Y.; Kunjir, S. M.; Banerjee, R. Phosphoric Acid Loaded Azo (-N=N-) Based Covalent Organic Framework for Proton Conduction. *J. Am. Chem. Soc.* **2014**, *136*, 6570–6573.
- (19) Zhu, Y.; Wan, S.; Jin, Y.; Zhang, W. Desymmetrized Vertex Design for the Synthesis of Covalent Organic Frameworks with Periodically Heterogeneous Pore Structures. J. Am. Chem. Soc. 2015, 137, 13772–13775.
- (20) Ohmori, O.; Kawano, M.; Fujita, M. A Two-in-One Crystal: Uptake of Two Different Guests into Two Distinct Channels of a Biporous Coordination Network. *Angew. Chem., Int. Ed.* **2005**, *44*, 1962–1964.
- (21) (a) Samori, P.; Rabe, J. P. Scanning Probe Microscopy Explorations on Conjugated (Macro)Molecular Architectures for Molecular Electronics. J. Phys. Condens. Matter 2002, 14, 9955-9973. (b) Barth, J. V.; Costantini, C.; Kern, K. Engineering Atomic and Molecular Nanostructures at Surfaces. Nature 2005, 437, 671-679. (c) Barth, J. V. Molecular Architectonic on Metal Surfaces. Annu. Rev. Phys. Chem. 2007, 58, 375-407. (d) Elemans, J. A. A. W.; Lei, S.; De Feyter, S. Molecular and Supramolecular Networks on Surfaces: From Two-Dimensional Crystal Engineering to Reactivity. Angew. Chem., Int. Ed. 2009, 48, 7298-7332. (e) Kudernac, T.; Lei, S.; Elemans, J. A. A. W.; De Feyter, S. Two-Dimensional Supramolecular Self-Assembly: Nanoporous Networks on Surfaces. Chem. Soc. Rev. 2009, 38, 402-421. (f) Bonifazi, D.; Mohnani, S.; Llanes-Pallas, A. Supramolecular Chemistry at Interfaces: Molecular Recognition on Nanopatterned Porous Surfaces. Chem. Eur. J. 2009, 15, 7004-7025. (g) Tobe, Y.; Tahara, K.; De Feyter, S. Adaptive Building Blocks Consisting of Rigid Triangular Core and Flexible Alkoxy Chains for Self-Assembly at Liquid/Solid Interfaces. Bull. Chem. Soc. Jpn. 2016, 89, 1277-1306.
- (22) Hisaki, I.; Nakagawa, S.; Tohnai, N.; Miyata, M. A C<sub>3</sub>-Symmetric Macrocycle-Based, Hydrogen-Bonded, Multiporous Hexagonal Network as a Motif of Porous Molecular Crystals. *Angew. Chem., Int. Ed.* **2015**, *54*, 3008–3012.
- (23) (a) Teyssandier, J.; De Feyter, S.; Mali, K. S. Host-Guest Chemistry in Two-Dimensional Supramolecular Networks. *Chem.*

- Commun. 2016, 52, 11465–11487. (b) Iritani, K.; Tahara, K.; De Feyter, S.; Tobe, Y. Host-Guest Chemistry in Integrated Porous Space Formed by Molecular Self-Assembly at Liquid-Solid Interfaces. Langmuir 2017, 33, 4601–4618.
- (24) Shen, Y.; Deng, K.; Yang, S.; Qin, B.; Cheng, S.; Zhu, N.; Ding, J.; Zhao, D.; Liu, J.; Zeng, Q.; Wang, C. Triangular-Shaped Molecular Random Tiling and Molecular Rotation in Two-Dimensional Glassy Networks. *Nanoscale* **2014**, *6*, 7221–7225.
- (25) Destoop, I.; Ghijsens, E.; Katayama, K.; Tahara, K.; Mali, K. S.; Tobe, Y.; De Feyter, S. Solvent-Induced Homochirality in Surface-Confined Low-Density Nanoporous Molecular Networks. *J. Am. Chem. Soc.* **2012**, *134*, 19568–19571.
- (26) Iritani, K.; Ikeda, M.; Yang, A.; Tahara, K.; Hirose, K.; Moore, J. S.; Tobe, Y. Hexagonal Molecular Tiling by Hexagonal Macrocycles at the Liquid/Solid Interface: Structural Effects on Packing Geometry. *Langmuir* **2017**, *33*, 12453–12462.
- (27) (a) Ryan, S. T. J.; Del Barrio, J.; Ghosh, I.; Biedermann, F.; Lazar, A. I.; Lan, Y.; Coulston, R. J.; Nau, W. M.; Scherman, O. A. Efficient Host-Guest Energy Transfer in Polycationic Cyclophane-Perylene Diimide Complexes in Water. J. Am. Chem. Soc. 2014, 136, 9053–9060. (b) Dale, E. J.; Vermeulen, N. A.; Juriček, M.; Barnes, J. C.; Young, R. M.; Wasielewski, M. R.; Stoddart, J. F. Supramolecular Explorations: Exhibiting the Extent of Extended Cationic Cyclophanes. Acc. Chem. Res. 2016, 49, 262–273. (c) Barnes, J. C.; Juriček, M.; Vermeulen, N. A.; Dale, E. J.; Stoddart, J. F. Synthesis of Ex<sup>n</sup>Box Cyclophanes. J. Org. Chem. 2013, 78, 11962–11969. (d) Anamimoghadam, O.; Cooper, J. A.; Nguyen, M. T.; Guo, Q.-H.; Mosca, L.; Roy, I.; Sun, J.; Stern, C. L.; Redfern, L.; Farha, O. K.; Stoddart, J. F. Cyclotris(paraquat-p-phenylenes). Angew. Chem., Int. Ed. 2019, 58, 13778–13783.
- (28) (a) Wilcox, C. S.; Glagovich, N. M.; Webb, T. H. Designing Synthetic Receptors for Shape-Selective Hydrophobic Binding. ACS Symp. Ser. 1994, 568, 282-290. (b) Webb, T. H.; Wilcox, C. S. Enantioselective and Diastereoselective Molecular Recognition of Neutral Molecules. Chem. Soc. Rev. 1993, 22, 383-395. (c) Diederich, F.; Dick, K. Inclusion Complexes between a Macrocyclic Host Molecule and Aromatic Hydrocarbon in Aqueous Solution. Angew. Chem., Int. Ed. Engl. 1983, 22, 715-716. (d) Diederich, F.; Dick, K. Spherical Host Molecules for the Complexation of Aromatic Hydrocarbons in Aqueous Solution. Angew. Chem., Int. Ed. Engl. 1984, 23, 810-812. (e) Diederich, F.; Dick, K. A New Water-Soluble Macrocyclic Host of the Cyclophane Type: Host-Guest Complexation with Aromatic Guests in Aqueous Solution and Acceleration of the Transport of Arenes through an Aqueous Phase. J. Am. Chem. Soc. 1984, 106, 8024-8036. (f) Gong, H.-Y.; Rambo, B. M.; Karnas, E.; Lynch, V. M.; Sessler, J. L. A 'Texas-Sized' Molecular Box that Forms an Anion-Induced Supramolecular Necklace. Nat. Chem. 2010, 2, 406-409. (g) Rambo, B. M.; Gong, H.-Y.; Oh, M.; Sessler, J. L. The "Texas-Sized" Molecular Box: A Versatile Building Block for the Construction of Anion-Directed Mechanically Interlocked Structures. Acc. Chem. Res. 2012, 45, 1390-1409.
- (29) (a) Habicher, T.; Diederich, F.; Gramlich, V. Catalytic Dendrophanes as Enzyme Mimics: Synthesis, Binding Properties, Micropolarity Effect, and Catalytic Activity of Dendritic Thiazolio-cyclophanes. *Helv. Chim. Acta* 1999, 82, 1066–1095. (b) Diederich, F.; Lutter, H.-D. Catalytic Cyclophanes: Supramolecular Catalysis of Benzoin Condensations by a Thiazolium Cyclophane. *J. Am. Chem. Soc.* 1989, 111, 8438–8446. (c) Ferreira, R. B.; Murray, L. J. Cyclophanes as Platforms for Reactive Multimetallic Complexes. *Acc. Chem. Res.* 2019, 52, 447–455.
- (30) (a) Roy, I.; Bobbala, S.; Young, R. M.; Beldjoudi, Y.; Nguyen, M. T.; Cetin, M. M.; Cooper, J. A.; Allen, S.; Anamimoghadam, O.; Scott, E. A.; Wasielewski, M. R.; Stoddart, J. F. A Supramolecular Approach for Modulated Photoprotection, Lysosomal Delivery, and Photodynamic Activity of a Photosensitizer. *J. Am. Chem. Soc.* 2019, 141, 12296—12304. (b) David, E.; Born, R.; Kaganer, E.; Joselevich, E.; Dürr, H.; Willner, I. Photoinduced Electron Transfer in Supramolecular Assemblies Composed of One-Shell and Two-Shell

- Dialkoxybenzene-Tethered Ru(II)-Tris(bipyridine) Derivatives and a Bipyridinium Cyclophane. J. Am. Chem. Soc. 1997, 119, 7778–7790. (31) (a) Luo, Y.; Collier, C. P.; Jeppesen, J. O.; Nielsen, K. A.; DeIonno, E.; Ho, G.; Perkins, J.; Tseng, H.-R.; Yamamoto, T.; Stoddart, J. F.; Heath, J. R. Two-Dimensional Molecular Electronics Circuits. ChemPhysChem 2002, 3, 519–525. (b) Kim, D. J.; Hermann, K. R.; Prokofjevs, A.; Otley, M. T.; Pezzato, C.; Owczarek, M.; Stoddart, J. F. Redox-Active Macrocycles for Organic Rechargeable Batteries. J. Am. Chem. Soc. 2017, 139, 6635–6643. (c) Fahrenbach, A. C.; Zhu, Z.; Cao, D.; Liu, W.-G.; Li, H.; Dey, S. K.; Basu, S.; Trabolsi, A.; Botros, Y. Y.; Goddard III, W. A.; Stoddart, J. F. Radically Enhanced Molecular Switches. J. Am. Chem. Soc. 2012, 134, 16275–16288.
- (32) Roy, I.; Bobbala, S.; Zhou, J.; Nguyen, M. T.; Nalluri, S. K. M.; Wu, Y.; Ferris, D. P.; Scott, E. A.; Wasielewski, M. R.; Stoddart, J. F. ExTzBox: A Glowing Cyclophane for Live-Cell Imaging. *J. Am. Chem. Soc.* 2018, 140, 7206–7212.
- (33) (a) McGlinchey, M. J.; Milosevic, S. From [10]Paracyclophane to Ferrocenophanones: The Search for Molecular Machines and Bio-Organometallic Anticancer Drugs. Isr. J. Chem. 2012, 52, 30–40. (b) Basheer, M. C.; Oka, Y.; Mathews, M.; Tamaoki, N. A Light-Controlled Molecular Brake with Complete ON-OFF Rotation. Chem. Eur. J. 2010, 16, 3489–3496. (c) Badjic, J. D.; Balzani, V.; Credi, A.; Silvi, S.; Stoddart, J. F. A Molecular Elevator. Science 2004, 303, 1845–1849. (d) Flood, A. M.; Liu, Y.; Stoddart, J. F. From Cyclophanes to Molecular Machines. Modern Cyclophane Chemistry; Wiley-VCH Verlag GmbH & Co. KGaA: Weinheim, 2005. (e) Bunker, B. C.; Huber, D. L.; Kushmerick, J. G.; Dunbar, T.; Kelly, M.; Matzke, C.; Cao, J.; Jeppesen, J. O.; Perkins, J.; Flood, A. H.; Stoddart, J. F. Switching Surface Chemistry with Supramolecular Machines. Langmuir 2007, 23, 31–34.
- (34) Beldjoudi, Y.; Narayanan, A.; Roy, I.; Pearson, T. J.; Cetin, M. M.; Nguyen, M. T.; Krzyaniak, M. D.; Alsubaie, F. M.; Wasielewski, M. R.; Stupp, S. I.; Stoddart, J. F. Supramolecular Tessellations by a Rigid Naphthalene Diimide Triangle. J. Am. Chem. Soc. 2019, 141, 17783—17795.
- (35) Yamamoto, S.; Pirillo, J.; Hijikata, Y.; Zhang, Z.; Awaga, K. Nanopore-Induced Host-Guest Charge Transfer Phenomena in a Metal-Organic Framework. *Chem. Sci.* **2018**, *9*, 3282–3289.
- (36) (a) Coskun, A.; Spruell, J. M.; Barin, G.; Fahrenbach, A. C.; Forgan, R. S.; Colvin, M. T.; Carmieli, R.; Bentez, D.; Tkatchouk, E.; Friedman, D. C.; Sarjeant, A. A.; Wasielewski, M. R.; Goddard III, W. A.; Stoddart, J. F. Mechanically Stabilized Tetrathiafulvalene Radical Dimers. J. Am. Chem. Soc. 2011, 133, 4538-4547. (b) Spruell, J. M.; Coskun, A.; Friedman, D. C.; Forgan, R. S.; Sarjeant, A. A.; Trabolsi, A.; Fahrenbach, A. C.; Barin, G.; Paxton, W. F.; Dey, S. K.; Olson, M. A.; Benítez, D.; Tkatchouk, E.; Colvin, M. T.; Carmielli, R.; Caldwell, S. T.; Rosair, G. M.; Hewage, S. G.; Duclairoir, F.; Seymour, J. L.; Slawin, A. M. Z.; Goddard III, W. A.; Wasielewski, M. R.; Cooke, G.; Stoddart, J. F. Highly Stable Tetrathiafulvalene Radical Dimers in [3] Catenanes. Nat. Chem. 2010, 2, 870-879. (c) Wang, C.; Dyar, S. M.; Cao, D.; Fahrenbach, A. C.; Horwitz, N.; Colvin, M. T.; Carmieli, R.; Stern, C. L.; Dey, S. K.; Wasielewski, M. R.; Stoddart, J. F. Tetrathiafulvalene Hetero Radical Cation Dimerization in a Redox-Active [2] Catenane. J. Am. Chem. Soc. 2012, 134, 19136-19145.
- (37) Peierls, R. E. Quantum Theory of Solids; Clarendon: Oxford, 1955.
- (38) (a) Umland, T. C.; Allie, S.; Kuhlmann, T.; Coppens, P. Relation between Geometry and Charge Transfer in Low-Dimensional Organic Salts. *J. Phys. Chem.* **1988**, 92, 6456–6460. (b) Guionneau, P.; Kepert, C. J.; Bravic, G.; Chasseau, D.; Truter, M. R.; Kurmoo, M.; Day, P. Determining the Charge Distribution in BEDT-TTF Salts. *Synth. Met.* **1997**, 86, 1973–1974.
- (39) Wartelle, C.; Viruela, R.; Viruela, P. M.; Sauvage, F. X.; Salle, M.; Orti, E.; Levillain, E.; Le Derf, F. First Signals of Electrochemically Oxidized Species of TTF and TTM-TTF: A Study by in situ Spectroelectrochemical FTIR and DFT Calculations. *Phys. Chem. Chem. Phys.* **2003**, *5*, 4672–4679.

- (40) Matsuzaki, S.; Kuwata, R.; Toyoda, K. Raman Spectra of Conducting TCNQ Salts; Estimation of the Degree of Charge Transfer from Vibrational Frequencies. *Solid State Commun.* **1980**, 33, 403–405.
- (41) Souto, M.; Lloveras, V.; Vela, S.; Fumanal, M.; Ratera, I.; Veciana, J. Three Redox States of a Diradical Acceptor-Donor-Acceptor Triad: Gating the Magnetic Coupling and the Electron Delocalization. *J. Phys. Chem. Lett.* **2016**, 7, 2234–2239. (b) Evans, H. A.; Labram, J. G.; Smock, S. R.; Wu, G.; Chabinyc, M. L.; Seshadri, S.; Wudl, F. Mono- and Mixed-Valence Tetrathiafulvalene Semi-conductors (TTF)BiI<sub>4</sub> and (TTF)<sub>4</sub>BiI<sub>6</sub> with 1D and 0D Bismuth-Iodide Networks. *Inorg. Chem.* **2017**, *56*, 395–401.
- (42) Jaguar, version 8.7; Schrodinger Inc.: New York, 2015. Bochevarov, A. D.; Harder, E.; Hughes, T. F.; Greenwood, J. R.; Braden, D. A.; Philipp, D. M.; Rinaldo, D.; Halls, M. D.; Zhang, J.; Friesner, R. A. Jaguar: A High-Performance Quantum Chemistry Software Program with Strengths in Life and Materials Sciences. Int. J. Quantum Chem. 2013, 113, 2110–2142.
- (43) Peon, J.; Tan, X.; Hoerner, J. D.; Xia, C.; Luk, Y. F.; Kohler, B. Excited State Dynamics of Methyl Viologen. Ultrafast Photoreduction in Methanol and Fluorescence in Acetonitrile. *J. Phys. Chem. A* **2001**, 105, 5768–5777.
- (44) (a) Santos, W. G.; Budkina, D. S.; Deflon, V. M.; Tarnovsky, A. N.; Cardoso, D. R.; Forbes, M. D. E. Photoinduced Charge Shifts and Electron Transfer in Viologen-Tetraphenylborate Complexes: Push-Pull Character of the Exciplex. *J. Am. Chem. Soc.* **2017**, *139*, 7681–7684.
- (45) Freitag, M.; Gundlach, L.; Piotrowiak, P.; Galoppini, E. Fluorescence Enhancement of Di-*p*-tolyl Viologen by Complexation in Cucurbit[7]uril. *J. Am. Chem. Soc.* **2012**, *134*, 3358–3366.
- (46) Benniston, A. C.; Harriman, A.; Li, P.; Rostron, J. P.; Harrington, R. W.; Clegg, W. A Spectroscopic Study of the Reduction of Geometrically Restrained Viologens. *Chem. Eur. J.* **2007**, *13*, 7838–7851.